

Phase structures of strong coupling lattice QCD with finite baryon and isospin density

Yusuke Nishida

Department of Physics, University of Tokyo, Tokyo 113-0033, Japan

(Dated: October 29, 2018)

Quantum chromodynamics (QCD) at finite temperature (T), baryon chemical potential (μ_B) and isospin chemical potential (μ_I) is studied in the strong coupling limit on a lattice with staggered fermions. With the use of large dimensional expansion and the mean field approximation, we derive an effective action written in terms of the chiral condensate and pion condensate as a function of T , μ_B and μ_I . The phase structure in the space of T and μ_B is elucidated, and simple analytical formulas for the critical line of the chiral phase transition and the tricritical point are derived. The effects of a finite quark mass (m) and finite μ_I on the phase diagram are discussed. We also investigate the phase structure in the space of T , μ_I and m , and clarify the correspondence between color SU(3) QCD with finite isospin density and color SU(2) QCD with finite baryon density. Comparisons of our results with those from recent Monte Carlo lattice simulations on finite density QCD are given.

I. INTRODUCTION

To reveal the nature of matter under extreme conditions in quantum chromodynamics (QCD) is one of the most interesting and challenging problems in hadron physics. At present the Relativistic Heavy Ion Collider (RHIC) experiments at Brookhaven National Laboratory are running in order to create a new state of hot matter, the quark-gluon plasma [1, 2]. On the other hand, various novel states of dense matter have been proposed at low temperature which are relevant to the physics of the interior of neutron star, such as the ${}^3\text{P}_2$ neutron superfluidity [3], the pion [4] and kaon [5] condensations and so on. Furthermore, if the baryon density reaches as much as ten times the nuclear density at the core of the neutron stars, quark matter in a color-superconducting state may be realized [6].

One of the first principles methods to solve QCD is numerical simulation on the basis of the Monte Carlo method. This has been successfully applied to study the chiral and deconfinement phase transitions at finite temperature ($T \neq 0$) with zero baryon chemical potential ($\mu_B = 0$) [7]. On the other hand, lattice QCD simulations have an intrinsic difficulty at finite μ_B due to the complex fermion determinant. Recently, new approaches have been proposed to attack the problem in SU_c(3) QCD at finite μ_B [8], such as the improved reweighting method [9], the Taylor expansion method around $\mu_B = 0$ [10] and analytic continuation from imaginary μ_B [11, 12]. They have indeed given us some idea about the phase structure of QCD, e.g., the existence of the critical end point of the chiral phase transition and the determination of the slope of the critical line. They are, however, inevitably restricted either to simulations on a small lattice volume or to the low μ_B region near the critical line. Alternative attempts have also been made to study theories with positive fermion determinant, which include color SU_c(2) QCD with finite μ_B [13, 14] and color SU_c(3) QCD with finite isospin chemical potential (μ_I) [15, 16].

In this paper we consider the strong coupling limit of SU_c(3) lattice QCD [17, 18, 19, 20, 21, 22] and make an extensive study of its phase structure with the use of the effective potential analytically calculated at finite T , μ_B , μ_I and the quark mass m . The phases obtained as functions of these variables are not easily accessible in Monte Carlo simulations and thus give us some insights into hot and dense QCD. Indeed, our previous study of strong coupling SU_c(2) QCD with finite T , μ_B and m show results which agree qualitatively well with those in numerical simulations [23]. Note that our approach has a closer connection to QCD than other complementary approaches based on the Nambu–Jona-Lasinio model [24], the random matrix model [25] and the Schwinger-Dyson method [26, 27].

This paper is organized as follows. In Sec. II, we consider color SU(N_c) QCD with finite temperature and baryon density. Starting from the lattice action in the strong coupling limit with one species of staggered fermion (corresponding to $N_f = 4$ flavors in the continuum limit), we derive an effective free energy in terms of a scalar mode σ and a pseudoscalar mode π for $N_c \geq 3$ using a large dimensional expansion and the mean field approximation (Sec. II A). The resultant free energy is simple enough that one can make analytical studies at least in the chiral limit $m = 0$ with finite T and μ_B . Section II B is devoted to such studies and useful formulas for the critical temperature and critical chemical potential for the chiral restoration are derived. In particular, we can present an analytical expression for the temperature and baryon chemical potential of the tricritical point. In Sec. II C, we analyze the chiral condensate and baryon density as functions of μ_B and show the phase diagram in the plane of T and μ_B for $N_c = 3, N_f = 4$. We discuss the effect of finite quark mass m on the phase diagram of QCD and comparison with the results from recent lattice simulations are given here.

In Sec. III, we consider the strong coupling lattice QCD with isospin chemical potential as well as T and μ_B . In order to include μ_I , we extend the formulation studied in Sec. II to two species of staggered fermion, which corresponds

to $N_f = 8$ flavor QCD in the continuum limit (Sec. III A). Then we restrict ourselves to two particular cases: One is at finite T , finite μ_B and *small* μ_I (Sec. III B); the other is at finite T , finite μ_I and *zero* μ_B (Sec. III C). For each case, we derive and analyze an analytical expression for the effective free energy and show the phase diagram in terms of T and μ_B or μ_I for $N_c = 3, N_f = 8$. In Sec. III B, we discuss the effect of increasing N_f and that of finite μ_I on the phase diagram of QCD in the T - μ_B plane. In Sec. III C, comparison with the results from lattice simulations and discussion of a correspondence between QCD with finite μ_I and $SU_c(2)$ QCD with finite μ_B are given. In Appendixes A and B, we give some technical details for deriving the effective free energy.

II. QCD ($N_c \geq 3, N_f = 4$) WITH FINITE BARYON DENSITY

In this section, we consider strong coupling lattice QCD with finite baryon density. First of all, we review how to derive the effective free energy written in terms of a scalar mode σ and a pseudoscalar mode π for $N_c \geq 3$ for further extension in Sec. III, while the resultant free energy is almost the same as that studied in [17, 18, 19]. Then we analyze the chiral phase transition in the chiral limit at finite temperature and density, and derive analytical formulas for the second order critical line and the tricritical point. Finally we show the phase diagram in terms of T and μ_B for $N_c = 3$.

A. Formulation of strong coupling lattice QCD

In order to derive the effective free energy written in terms of the scalar and pseudoscalar modes, we start from the lattice action with one species of staggered fermion, which corresponds to the continuum QCD with four flavors. In the strong coupling limit, the gluonic part of the action vanishes because it is inversely proportional to the square of the gauge coupling constant g . Consequently, the lattice action in the strong coupling limit is given by only the fermionic part:

$$S[U, \chi, \bar{\chi}] = m \sum_x \bar{\chi}(x)\chi(x) + \frac{1}{2} \sum_x \eta_0(x) \left\{ \bar{\chi}(x)e^{\mu}U_0(x)\chi(x + \hat{0}) - \bar{\chi}(x + \hat{0})e^{-\mu}U_0^\dagger(x)\chi(x) \right\} \\ + \frac{1}{2} \sum_x \sum_{j=1}^d \eta_j(x) \left\{ \bar{\chi}(x)U_j(x)\chi(x + \hat{j}) - \bar{\chi}(x + \hat{j})U_j^\dagger(x)\chi(x) \right\}. \quad (1)$$

χ stands for the quark field in the fundamental representation of the color $SU(N_c)$ group and U_μ is the $SU(N_c)$ valued gauge link variable. d represents the number of spatial directions and we use a notation $x = (\tau, \vec{x})$ in which τ (\vec{x}) represents the temporal (spatial) coordinate. $\eta_0(x)$ and $\eta_j(x)$ inherent in the staggered formalism are defined as $\eta_0(x) = 1$, $\eta_j(x) = (-1)^{\sum_{i=1}^j x_{i-1}}$. μ is the quark chemical potential, while the temperature is defined by $T = (aN_\tau)^{-1}$ with a being the lattice spacing and N_τ being the number of temporal sites. We will write all the dimensionful quantities in units of a and will not write a explicitly.

This lattice action has $U(1)_V \times U(1)_A$ symmetry in the chiral limit $m = 0$, which is a remnant of the four flavor chiral symmetry in the continuum theory, defined by $U(1)_V : \chi(x) \mapsto e^{i\theta_V}\chi(x)$, $\bar{\chi}(x) \mapsto \bar{\chi}(x)e^{-i\theta_V}$ and $U(1)_A : \chi(x) \mapsto e^{i\varepsilon(x)\theta_A}\chi(x)$, $\bar{\chi}(x) \mapsto \bar{\chi}(x)e^{i\varepsilon(x)\theta_A}$. Here $\varepsilon(x)$ is given by $\varepsilon(x) = (-1)^{\sum_{\nu=0}^d x_\nu}$, which plays a similar role to γ_5 in the continuum theory. $U(1)_A$ will be explicitly broken by the introduction of a finite quark mass or spontaneously broken by condensation of $\langle \bar{\chi}\chi \rangle$. Note that the staggered fermion's $U(1)_A$ symmetry should not be confused with the axial $U(1)$ symmetry in the continuum theory, which is broken by the quantum effect. Now by using the lattice action Eq. (1), we can write the partition function as

$$Z = \int \mathcal{D}[\chi, \bar{\chi}] \mathcal{D}[U_0] \mathcal{D}[U_j] e^{-S}. \quad (2)$$

In the succeeding part of this subsection, we perform the path integrals by use of the large dimensional ($1/d$) expansion and the mean field approximation to derive the effective free energy.

First, we perform the integration over spatial gauge link variable U_j using the formulas for the $SU(N_c)$ group integration. Keeping only the lowest order term of the Taylor expansion of e^{-S} , which corresponds to the leading

order term of the $1/d$ expansion [28], we can calculate the group integral as follows:

$$\int \mathcal{D}[U_j] \exp \left[-\frac{1}{2} \sum_x \sum_{j=1}^d \eta_j(x) \left\{ \bar{\chi}(x) U_j(x) \chi(x + \hat{j}) - \bar{\chi}(x + \hat{j}) U_j^\dagger(x) \chi(x) \right\} \right] = \exp \left[\sum_{x,y} M(x) V_M(x,y) M(y) \right] + \dots, \quad (3)$$

where $M(x)$ and $V_M(x,y)$ are the mesonic composite and its propagator in the spatial dimensions, defined, respectively, by

$$M(x) = \frac{1}{N_c} \delta_{ab} \bar{\chi}^a(x) \chi^b(x), \quad V_M(x,y) = \frac{N_c}{8} \sum_{j=1}^d \left(\delta_{y,x+\hat{j}} + \delta_{y,x-\hat{j}} \right). \quad (4)$$

The resultant term in the action describes the nearest neighbor interaction of the mesonic composite $M(x)$. Residual terms are in higher order of the $1/d$ expansion and vanish in the large dimensional limit. Note that Eq. (3) is correct as long as $N_c \geq 3$. For $N_c = 2$ the baryonic composite (diquark field) gives the same contribution as the mesonic one in the $1/d$ expansion. The finite density $SU_c(2)$ QCD with a diquark field was studied in a previous paper [23].

Next, we linearize the four-fermion term in Eq. (3) by introduction of the auxiliary field $\sigma(x)$. This is accomplished by the standard Gaussian technique;

$$\exp \left[\sum_{x,y} M(x) V_M(x,y) M(y) \right] = \int \mathcal{D}[\sigma] \exp \left[-\sum_{x,y} \{ \sigma(x) V_M(x,y) \sigma(y) + 2\sigma(x) V_M(x,y) M(y) \} \right]. \quad (5)$$

From the above transformation, we can show the relation between the vacuum expectation values of the auxiliary field and the mesonic composite: $\langle \sigma(x) \rangle = -\langle M(x) \rangle$. In order to keep the action invariant under the $U(1)_V$ and $U(1)_A$ transformations, we should assign the transformation for the auxiliary field as $U(1)_V : \sigma(x) \mapsto \sigma(x)$ and $U(1)_A : \sigma(x) \mapsto e^{2i\varepsilon(x)\theta_A} \sigma(x)$.

In the staggered fermion formalism, one species of staggered fermion at various sites is responsible for the degree of freedom of flavors and spins. Therefore the auxiliary field $\sigma(x)$ is responsible for both the scalar mode σ and the pseudoscalar mode π [28]. In order to derive the effective free energy written using the scalar and pseudoscalar modes, we introduce σ and π as $\sigma(x) = \sigma + i\varepsilon(x)\pi$ [29]. Then we can find a correspondence between these new values σ , π and the vacuum expectation values of the mesonic composites: $\sigma = -\langle \bar{\chi}^a(x) \chi^a(x) \rangle / N_c$, $\pi = \langle i \bar{\chi}^a(x) \varepsilon(x) \chi^a(x) \rangle / N_c$. These equations tell us that σ and π are even and odd under lattice parity, respectively [13, 30], and therefore σ and π correspond to the spatially uniform condensates of the scalar mode (chiral condensate) and the pseudoscalar mode (pion condensate). They transform under $U(1)_A$ transformation as

$$U(1)_A : \begin{pmatrix} \sigma \\ \pi \end{pmatrix} \mapsto \begin{pmatrix} \cos 2\theta_A & -\sin 2\theta_A \\ \sin 2\theta_A & \cos 2\theta_A \end{pmatrix} \begin{pmatrix} \sigma \\ \pi \end{pmatrix}. \quad (6)$$

The partition function is then written as

$$Z = \int \mathcal{D}[U_0] \mathcal{D}[\chi, \bar{\chi}] e^{-S'[U_0, \chi, \bar{\chi}; \sigma, \pi]}, \quad (7)$$

with

$$S'[U_0, \chi, \bar{\chi}; \sigma, \pi] = \sum_x \left[m \bar{\chi}(x) \chi(x) + \frac{1}{2} \left\{ \bar{\chi}(x) e^{\mu} U_0(x) \chi(x + \hat{0}) - \bar{\chi}(x + \hat{0}) e^{-\mu} U_0^\dagger(x) \chi(x) \right\} + \frac{N_c d}{4} (\sigma^2 + \pi^2) + \frac{N_c d}{2} \{ \sigma - i\varepsilon(x)\pi \} M(x) \right]. \quad (8)$$

Note that this action contains hopping terms of χ , $\bar{\chi}$ only in the temporal direction after the $1/d$ expansion and the mean field approximation.

In order to complete the remaining integrals, we adopt the Polyakov gauge [17] in which $U_0(\tau, \vec{x})$ is diagonal and independent of τ :

$$U_0(\tau, \vec{x}) = \text{diag} \left[e^{i\phi_1(\vec{x})/N_\tau}, \dots, e^{i\phi_{N_c}(\vec{x})/N_\tau} \right] \quad \text{with} \quad \sum_{a=1}^{N_c} \phi_a(\vec{x}) = 0. \quad (9)$$

Also we make a partial Fourier transformation for the quark fields;

$$\chi(\tau, \vec{x}) = \frac{1}{\sqrt{N_\tau}} \sum_{n=1}^{N_\tau} e^{ik_n \tau} \tilde{\chi}(n, \vec{x}), \quad \bar{\chi}(\tau, \vec{x}) = \frac{1}{\sqrt{N_\tau}} \sum_{n=1}^{N_\tau} e^{-ik_n \tau} \tilde{\bar{\chi}}(n, \vec{x}), \quad k_n = 2\pi \frac{(n - \frac{1}{2})}{N_\tau}. \quad (10)$$

Substituting Eqs. (9) and (10) into the action (8) and taking the summation over τ , the Grassmann integration over the the quark fields $\tilde{\chi}$ and $\tilde{\bar{\chi}}$ results in the following determinant:

$$\prod_{\vec{x}} \prod_{a=1}^{N_c} \prod_{n=1}^{N_\tau/2} \left[\sin^2 \bar{k}_n + M^2 + \left(\frac{d}{2} \pi \right)^2 \right] \quad (11)$$

with $\bar{k}_n = k_n + \phi_a(\vec{x})/N_\tau - i\mu$. M denotes the dynamical quark mass defined by $M = m + (d/2)\sigma$.

The product with respect to the Matsubara frequencies n can be performed using a technique similar to that in the calculation of the free energy in finite temperature continuum field theory. The details of the calculation are given in Appendix A. The result turns out to have a quite simple form: $2 \cosh[N_\tau E] + 2 \cos[\phi_a(\vec{x}) - iN_\tau \mu]$ with one-dimensional quark excitation energy $E[\sigma, \pi] = \text{arcsinh}[\sqrt{M^2 + (d/2)^2 \pi^2}]$.

Finally we can perform the integration with respect to U_0 by use of the formula in Appendix B for the Polyakov gauge. Then the integration gives, up to an irrelevant factor,

$$\int \mathcal{D}[U_0] \prod_{\vec{x}} \prod_{a=1}^{N_c} \{2 \cosh[N_\tau E] + 2 \cos[\phi_a(\vec{x}) - iN_\tau \mu]\} = \prod_{\vec{x}} \left\{ \sum_n \det_{i,j} P_{n+i-j} \right\}, \quad (12)$$

where $P_0 = 2 \cosh[N_\tau E]$, $P_{\pm 1} = \cosh[N_\tau \mu] \pm \sinh[N_\tau \mu] = e^{\pm N_\tau \mu}$ and $P_{|n| \geq 3} = 0$. The determinant is to be taken with respect to $i, j = 1, 2, \dots, N_c$. The determinants have nonvanishing values only for $n = 0, \pm 1$ and their summation can be calculated exactly for general N_c . First, for $n = 0$, $\det P_{i-j}$ is expressed in the form of an $N_c \times N_c$ matrix as

$$\det_{i,j} P_{i-j} = \begin{vmatrix} P_0 & P_{-1} & 0 & \cdots \\ P_{+1} & P_0 & \ddots & \\ 0 & \ddots & \ddots & P_{-1} \\ \vdots & & P_{+1} & P_0 \end{vmatrix}. \quad (13)$$

Making a recursion formula for it and using the fact that $P_{-1}P_{+1} = 1$, we can obtain the simple solution $\det P_{i-j} = \sinh[(N_c + 1)N_\tau E] / \sinh[N_\tau E]$ [17]. Then the calculation for $n = \pm 1$ is rather easy and results in $\det P_{-1+i-j} + \det P_{1+i-j} = P_{-1}^{N_c} + P_{+1}^{N_c} = 2 \cosh[N_c N_\tau \mu]$. As a result, the effective free energy is given as follows;

$$F_{\text{eff}}[\sigma, \pi; T, \mu_B] = (-\log Z) / (\sum_x) = \frac{N_c d}{4} (\sigma^2 + \pi^2) - T \log \left\{ 2 \cosh[\mu_B/T] + \frac{\sinh[(N_c + 1)E/T]}{\sinh[E/T]} \right\}. \quad (14)$$

Here we have defined the baryon chemical potential μ_B as $\mu_B = N_c \mu$. Although the temperature $T = 1/N_\tau$ takes discrete values, the effective free energy $F_{\text{eff}}[1/N_\tau]$ can be uniquely extended to a function of continuous T in terms of an analytic continuation since $F_{\text{eff}}[1/N_\tau]$ is defined on an infinite sequence of points. Hereafter we consider T as a continuous variable. This effective free energy in Eq. (14) corresponds to the $N_f = 4$ flavor QCD in the continuum limit.

B. Analytical properties in the chiral limit

The effective free energy obtained in the previous subsection is simple enough to make analytical studies in the chiral limit. This is one of the main advantages of our approach. Such analytical studies on the chiral phase transition are useful in understanding the phase structure of strong coupling lattice QCD, which will be presented in the next subsection. In the chiral limit $m = 0$, the quark excitation energy reduces to $E[\sigma, \pi] = \text{arcsinh}[(d/2)\sqrt{\sigma^2 + \pi^2}]$. Therefore the effective free energy in Eq. (14) is a function of only $\sqrt{\sigma^2 + \pi^2}$. Of course this symmetry comes from the chiral symmetry $U(1)_A$ of the original lattice action. Since we can arbitrarily choose the direction of the condensate, we take $\sigma \neq 0$ and $\pi = 0$.

Chiral restoration at finite temperature

As we will confirm numerically in the next subsection, the effective free energy exhibits a second order phase transition at finite temperature. Therefore we can expand it in terms of the order parameter σ near the critical point. Expansion of the effective free energy up to second order of the chiral condensate σ gives

$$F_{\text{eff}}[\sigma, 0] = \frac{N_c d}{4} \sigma^2 - \frac{d^2 N_c (N_c + 1)(N_c + 2)}{24T(N_c + 1 + 2 \cosh[\mu_B/T])} \sigma^2 + O(\sigma^4). \quad (15)$$

As long as the coefficient of σ^4 is positive, the condition that the coefficient of σ^2 is zero gives the critical chemical potential for the second order phase transition as a function of temperature:

$$\mu_B^{\text{cri}}(T) = T \operatorname{arccosh} \left[\frac{(N_c + 1)\{d(N_c + 2) - 6T\}}{12T} \right]. \quad (16)$$

The critical temperature at zero chemical potential is given by solving the equation $\mu_B^{\text{cri}}(T) = 0$ and turns out to be $T_c(0) = d(N_c + 1)(N_c + 2)/[6(N_c + 3)]$.

When the coefficient of σ^4 becomes zero, the phase transition becomes of first order. An analytical expression for the tricritical point $(T_{\text{tri}}, \mu_{\text{tri}})$ can be obtained as a solution of the coupled equations of Eq. (16) and $\partial^4 F_{\text{eff}}/\partial \sigma^4 = 0$, which results in

$$T_{\text{tri}} = \frac{\sqrt{225N_c^2 + 20d^2(3N_c^2 + 6N_c - 4)} - 15N_c}{20d}, \quad \mu_{\text{tri}} = \mu_B^{\text{cri}}(T_{\text{tri}}). \quad (17)$$

The effective free energy exhibits a second order chiral phase transition for $T \geq T_{\text{tri}}$ and it becomes of first order for $T < T_{\text{tri}}$. The existence of the tricritical point is consistent with the results of other analytical approaches using the Nambu–Jona-Lasinio model [24], random matrix model [25], Schwinger-Dyson equation [26] and other methods [27, 31, 32].

Chiral restoration at finite density

An analytical study of the first order chiral phase transition at finite temperature for $T < T_{\text{tri}}$ is rather involved. However, the effective free energy reduces to a simpler form at $T = 0$:

$$F_{\text{eff}}[T = 0] = \frac{N_c d}{4} \sigma^2 - \max\{\mu_B, N_c E[\sigma]\}, \quad E[\sigma] = \operatorname{arcsinh} \left[\frac{d}{2} |\sigma| \right]. \quad (18)$$

It is easy to study the first order phase transition analytically in this case.

The effective free energy has two local minima as a function of σ : One is $F_{\text{eff}} = -\mu_B$ at $\sigma = 0$; the other is $F_{\text{eff}} = N_c d \sigma_0^2/4 - N_c E[\sigma_0] < 0$ at $\sigma = \sigma_0$, where σ_0 is the solution of the chiral gap equation $\partial F_{\text{eff}}/\partial \sigma = 0$,

$$\sigma_0^2 \left[1 + \left(\frac{d}{2} \sigma_0 \right)^2 \right] = 1, \quad \text{therefore} \quad \sigma_0^2 = \frac{2\sqrt{1 + d^2} - 2}{d^2}. \quad (19)$$

As μ_B becomes larger, the global minimum changes from $N_c d \sigma_0^2/4 - N_c E[\sigma_0]$ to $-\mu_B$ at some value of the chemical potential. This is the critical chemical potential, given by $\mu_B^{\text{cri}}(T = 0) = N_c E[\sigma_0] - N_c d \sigma_0^2/4$. At this critical point, the order parameter σ changes discontinuously as

$$\sigma(\mu) = \begin{cases} \sigma_0 & \text{when } \mu_B < \mu_B^{\text{cri}}, \\ 0 & \text{when } \mu_B > \mu_B^{\text{cri}}. \end{cases} \quad (20)$$

This is a first order phase transition. We can also easily calculate the baryon density ρ_B at $T = 0$, and it has a discontinuity associated with that of the chiral condensate:

$$\rho_B = -\frac{\partial F_{\text{eff}}}{\partial \mu_B} = \begin{cases} 0 & \text{when } \mu_B < \mu_B^{\text{cri}}, \\ 1 & \text{when } \mu_B > \mu_B^{\text{cri}}. \end{cases} \quad (21)$$

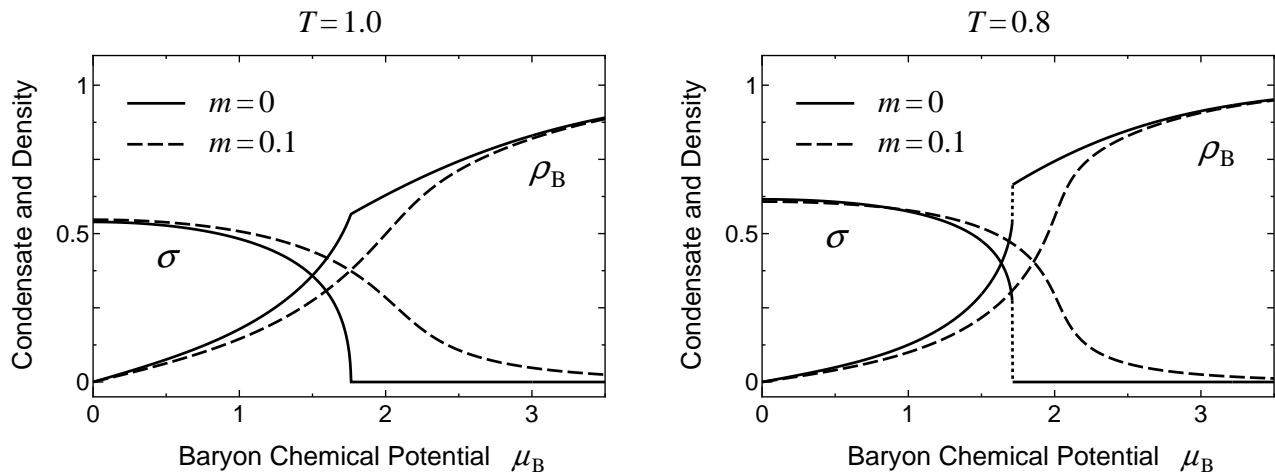


FIG. 1: Chiral condensate σ and baryon density ρ_B as functions of the baryon chemical potential μ_B for $N_c = 3, N_f = 4$. In the left panel, they are plotted just above the tricritical temperature ($T_{\text{tri}} = 0.866$) at $T = 1.0$ for $m = 0$ (the solid line) and $m = 0.1$ (the dashed one). In the right panel, they are plotted just below T_{tri} at $T = 0.8$ for $m = 0$ (the solid line) and $m = 0.1$ (the dashed one).

At the critical chemical potential, ρ_B changes from the empty density 0 to the saturated density 1 [20]. Note that one baryon ($= N_c$ quarks) at one lattice site, that is $\rho_B = 1$, is the maximally allowed configuration by the Fermi statistics for one species of staggered fermion. Saturation at large chemical potential on the lattice has also been observed in lattice simulations and strong coupling analyses of $SU_c(2)$ QCD [14, 23].

This chiral phase transition with finite μ_B at $T = 0$ is not associated with the deconfinement phase transition to quark matter. Equations (20) and (21) show that the chiral restoration coincides with the transition from vacuum to saturated nuclear matter, although they are in general separated [25]. Including the contribution of dynamical baryons, which is suppressed in the leading order of the $1/d$ expansion, will introduce the Fermi surface of baryons and hence separate the two phase transitions.

C. The phase structure with finite quark mass

In this subsection, setting the number of colors and spatial dimensions to 3, we examine numerically the nature of the chiral phase transition and the phase diagram of strong coupling lattice QCD for $N_c = 3, N_f = 4$.

Chiral condensate and baryon density

By minimizing the effective free energy F_{eff} for $N_c = 3, d = 3$ in terms of the order parameter σ , we determine the chiral condensate as a function of T and μ_B . The baryon density ρ_B is also calculated by $-\partial F_{\text{eff}}/\partial \mu_B$. In Fig. 1, the results with zero and finite m are shown as functions of μ_B .

In the left panel of Fig. 1, σ and μ_B are shown for $T = 1.0$ just above $T_{\text{tri}} = 0.866$. In the chiral limit they show a second order phase transition at the critical chemical potential given by Eq. (16), while introduction of an infinitesimal m makes the transition a smooth crossover.

σ and μ_B are shown for $T = 0.8$ just below T_{tri} in the right panel of Fig. 1. As discussed in the previous subsection, they show jumps at the critical chemical potential in the chiral limit. This first order phase transition is weakened by the introduction of m and finally becomes a crossover for large quark masses.

The phase diagram

Now we show in Fig. 2 the phase diagram of the strong coupling lattice QCD with $N_c = 3, N_f = 4$ in the plane of T and μ_B . In the chiral limit, the chiral condensate σ has nonvanishing value at low T and small μ_B , which means a spontaneous breakdown of the chiral symmetry $U_A(1)$ by the condensation $\sigma \neq 0$. The symmetry broken phase

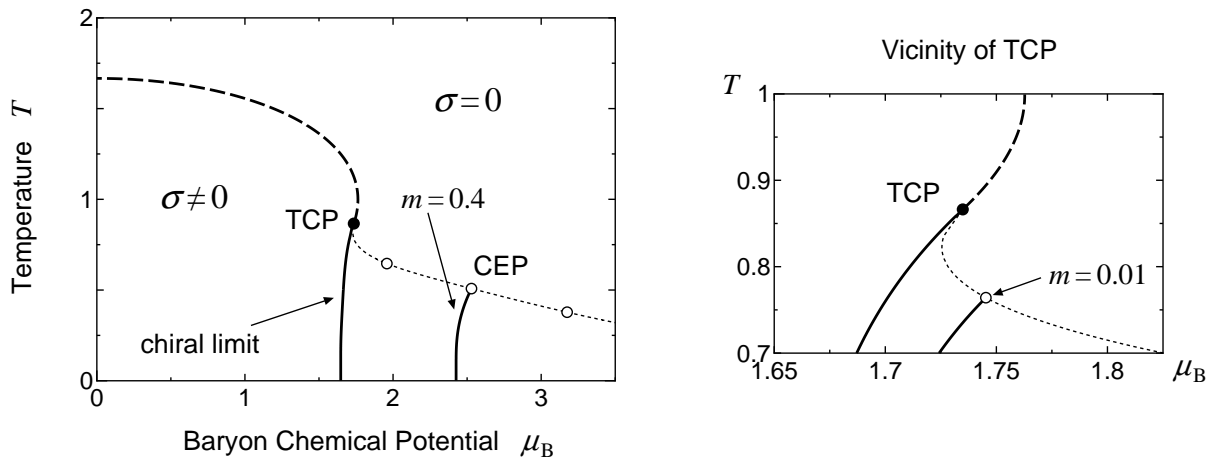


FIG. 2: Phase diagram of strong coupling lattice QCD with $N_c = 3$, $N_f = 4$ in the T - μ_B plane. The solid (dashed) line denotes the phase transition line for the first (second) order phase transition in the chiral limit. The black circle represents the tricritical point (TCP) where the nature of the phase transition changes from first order to second. The first order line and its critical end point (CEP) for $m = 0.4$ are also shown. The dotted line denotes the flow of the critical end points when the quark mass is enlarged from 0. White circles are put on the critical end points for $m = 0.1$ (the left one), $m = 0.4$ (the middle) and $m = 0.8$ (the right one) in the left panel. The vicinity of the TCP is enlarged and the first order line and CEP for $m = 0.01$ are shown in the right panel.

is separated by a phase transition from the chiral symmetric phase; the phase transition is of second order in the high temperature region while it is of first order in the low temperature region. The second order critical line merges smoothly into the first order one at the tricritical point $(T_{\text{tri}}, \mu_{\text{tri}}) = (0.866, 1.73)$.

In contradiction to our result, the chiral phase transition of four-flavor QCD in the chiral limit is thought to be of first order [9, 12]. This difference comes from the fact that the symmetry of the staggered fermion action is limited to $U(1) \times U(1)$ in the strong coupling limit and we have employed the mean field approximation.¹ However, it is sensible to consider that the second order critical line in our result corresponds to the phase transition line of chiral restoration in QCD.

As we can see from Fig. 2, the critical temperature falls much more rapidly as a function of μ_B in contrast to the results from recent Monte Carlo simulations at small chemical potential [9, 10, 11, 12]. In order to make the discussion quantitative, we calculate the slope of the critical temperature near zero chemical potential. From Eq. (16),

$$\frac{T_c(\mu)}{T_c(0)} = 1 - 1.5 \frac{\mu^2}{T_c(0)^2} - 3.375 \frac{\mu^4}{T_c(0)^4} + O\left(\left(\frac{\mu}{T_c}\right)^6\right) \quad (22)$$

with $T_c(0) = 5/3$. Here we have written Eq. (22) in terms of the quark chemical potential $\mu = \mu_B/N_c$ in order to make the comparison to the lattice data easy. The value of the coefficient of the second term is two orders of magnitude larger than that calculated in the lattice simulation with $N_f = 4$ for $m = 0.05$ [12]. This large difference in the slope of the chiral phase transition may be understood due to the effect of $m = 0$ and that of $g \rightarrow \infty$. Our expression (22) is derived in the chiral limit, while all of the lattice simulations are performed with finite quark mass. As reported in [34], the chiral transition line has significant quark mass dependence in the lattice simulations: The slope of $T_c(\mu)$ suffers a sharp increase on decreasing m , from 0.025 ($m = 0.1$) to 0.114 ($m = 0.005$) in $N_f = 3$ QCD. In addition to that, as we can find in [19], the introduction of the next to leading order term of $1/g^2$ and $1/d$ in strong coupling lattice QCD decreases the critical temperature, and the amount of decrease at zero chemical potential is more than that at finite chemical potential. Therefore the slope of the critical temperature will be made softer by the corrections for the strong coupling and large dimensional expansions. Combining the above two effects, the difference of the slope between our result and lattice simulations could become reasonably small; this needs further study.

Next we consider the effect of quark mass on the phase diagram. Introduction of finite m washes out the second order phase transition as shown in the left panel of Fig. 1. As a result, the first order phase transition line terminates

¹ As one gets closer to the continuum limit, the symmetry will turn into the usual four-flavor chiral symmetry. Then the chiral fluctuations may induce a first order phase transition, as they do in the corresponding linear sigma model [33].

TABLE I: Tricritical point $(T_{\text{tri}}, \mu_{\text{tri}})$ for $m = 0$ and critical end points $(T_{\text{end}}, \mu_{\text{end}})$ for various small quark masses. The deviations of the critical end points from the tricritical point are also shown.

m	T_{end}	μ_{end}	$(T_{\text{end}} - T_{\text{tri}})/T_{\text{tri}}$	$(\mu_{\text{end}} - \mu_{\text{tri}})/\mu_{\text{tri}}$
0	0.866	1.73	—	—
0.001	0.823	1.73	-5.03 %	-0.541 %
0.01	0.764	1.75	-11.8 %	0.599 %
0.05	0.690	1.85	-20.4 %	6.37 %
0.1	0.646	1.96	-25.5 %	12.9 %
0.2	0.590	2.16	-31.9 %	24.7 %

at a second order critical end point $(T_{\text{end}}, \mu_{\text{end}})$. As long as the quark mass is very small, $m \lesssim 0.001$, the critical end point flows almost along the tangent line at the tricritical point as in the right panel of Fig. 2. Then for the larger quark mass $m \gtrsim 0.001$, T_{end} decreases and μ_{end} increases. Also, the first order phase transition line shifts in the direction of large μ_{B} associated with this change.

Strong coupling lattice QCD may give us some indication for lattice simulations about the effect of m on the phase diagram of QCD. As shown in Table I, a finite quark mass $m = 0.1$ decreases T_{end} by 25% and increases μ_{end} by 12% from the tricritical point $(T_{\text{tri}}, \mu_{\text{tri}})$. We can find in the same way that even a quark mass as small as $m = 0.001$ can move the critical end point by 5%. This indicates the relatively large dependence of the phase diagram of QCD on the quark mass.

Our phase structure is consistent with those from other analytical approaches [24, 25, 26, 27, 31, 32], except for one main difference [22]. This is the fact that the gradient of the phase transition line near the tricritical point or critical end point is positive. Consequently, the critical end point flows in the direction of smaller T and smaller μ_{B} as a function of small quark mass. The positive gradient of the chiral phase transition line near the tricritical point can be understood as follows. The gradient $dT/d\mu$ is related to discontinuities in baryon density $\Delta\rho$ and in entropy density Δs across the phase boundary through the generalized Clapeyron-Clausius relation [25]

$$\frac{dT}{d\mu} = -\frac{\Delta\rho}{\Delta s}. \quad (23)$$

As we can see in the right panel of Fig. 1, the baryon density in the chiral restored phase ρ_+ is larger than that in the chiral broken phase ρ_- just below the tricritical point ($T = 0.8, \mu_{\text{B}} = 1.7$). We can also calculate the entropy density from the effective free energy (14) showing the result that $\Delta s < 0$. $\Delta\rho = \rho_+ - \rho_- > 0$ holds because baryons are massless in the chiral restored phase and we can fill more baryons under fixed μ_{B} . Since we are in the leading order of the $1/d$ expansion, all baryons are static. Then we can estimate the entropy as $s_{\pm} \sim -\rho_{\pm} \log \rho_{\pm} - (1 - \rho_{\pm}) \log(1 - \rho_{\pm})$. Because $1 > \rho_+ > \rho_- > 0.5$, the discontinuities in the entropy density is negative $\Delta s = s_+ - s_- < 0$. Therefore the gradient of the chiral phase transition line just below the tricritical point turns out to be positive, $dT/d\mu = -\Delta\rho/\Delta s > 0$.

III. QCD ($N_c \geq 3, N_f = 8$) WITH FINITE ISOSPIN DENSITY

In this section, we consider strong coupling lattice QCD with finite isospin density. First of all, we derive the analytical expression for the effective free energy in two particular cases. One is at finite T , finite μ_{B} and *small* μ_{I} with chiral condensates. The other is at finite T , finite μ_{I} and *zero* μ_{B} with chiral and pion condensates. Then we analyze the effective free energy and show the phase diagrams in terms of T and μ_{B} or μ_{I} for $N_c = 3, N_f = 8$.

A. Strong coupling lattice QCD with isospin chemical potential

In order to investigate the effect of the isospin chemical potential μ_{I} on the phase structure of QCD, we have to extend the lattice action studied in the previous section to that with two species of staggered fermion having degenerate masses. The lattice action with two species of staggered fermion corresponds to the eight-flavor QCD in the continuum limit. Then for $m = 0$ and $\mu_{\text{I}} = 0$, it has $U(2)_{\text{V}} \times U(2)_{\text{A}}$ symmetry, as a remnant of eight-flavor chiral symmetry, defined by $\chi(x) \mapsto e^{i[\theta_{\text{V}} + \varepsilon(x)\theta_{\text{A}}] \cdot \tau} \chi(x)$ and $\bar{\chi}(x) \mapsto \bar{\chi}(x) e^{-i[\theta_{\text{V}} - \varepsilon(x)\theta_{\text{A}}] \cdot \tau}$ with $\tau \in U(2)$.

After integrating out the spatial link variable U_j in the leading order of $1/d$ expansion and introducing the auxiliary fields, we have the following partition function:

$$Z = \int \mathcal{D}[U_0] \mathcal{D}[\chi, \bar{\chi}] \mathcal{D}[\sigma] e^{-S'[U_0, \chi, \bar{\chi}; \sigma]}, \quad (24)$$

with

$$\begin{aligned} S'[U_0, \chi, \bar{\chi}; \sigma] = & \sum_{\alpha=u,d} \sum_{x,y} \bar{\chi}_\alpha(x) \left[m\delta_{x,y} + \frac{1}{2} \left\{ e^{\mu_\alpha} U_0(x) \delta_{y,x+\hat{0}} - e^{-\mu_\alpha} U_0^\dagger(x) \delta_{y,x-\hat{0}} \right\} \right] \chi_\alpha(y) \\ & + \sum_{\alpha,\beta=u,d} \sum_{x,y} [\sigma_{\beta\alpha}(x) V_M(x,y) \sigma_{\alpha\beta}(y) + 2\sigma_{\beta\alpha}(x) V_M(x,y) M_{\alpha\beta}(y)]. \end{aligned} \quad (25)$$

Here the subscripts α, β represent the species of staggered fermion, taking ‘‘u’’ (for up quarks) and ‘‘d’’ (for down quarks). μ_u, μ_d are the quark chemical potentials for each species of staggered fermion. $\sigma_{\alpha\beta}(x)$ are auxiliary fields for the mesonic composites $M_{\alpha\beta}(x) = \bar{\chi}_\alpha^a(x) \chi_\beta^a(x) / N_c$, and these vacuum expectation values read $\langle \sigma_{\alpha\beta}(x) \rangle = -\langle M_{\alpha\beta}(x) \rangle$.

Now we replace the auxiliary fields $\sigma_{uu}(x)$ and $\sigma_{dd}(x)$ by spatially uniform condensates of the scalar mode as $\sigma_{uu}(x) = \sigma_u$, $\sigma_{dd}(x) = \sigma_d$. Then we find that σ_u and σ_d correspond to the chiral condensates of the up and down quarks: $\sigma_u = -\langle \bar{u}^a(x) u^a(x) \rangle / N_c$ and $\sigma_d = -\langle \bar{d}^a(x) d^a(x) \rangle / N_c$. We also replace $\sigma_{ud}(x)$ and $\sigma_{du}(x)$ by spatially uniform condensates of the pseudoscalar mode as $\sigma_{ud}(x) = i\varepsilon(x)\pi$, $\sigma_{du}(x) = i\varepsilon(x)\pi^*$. Then π corresponds to the charged pion condensates: $\pi = \langle i\bar{u}^a(x)\varepsilon(x)d^a(x) \rangle / N_c$ and $\pi^* = \langle i\bar{d}^a(x)\varepsilon(x)u^a(x) \rangle / N_c$.

Substituting these mean field values and Eqs. (9), (10) in the action (25), we obtain

$$S'[\phi, \chi, \bar{\chi}; \sigma_u, \sigma_d, \pi] = \sum_x \frac{N_c d}{4} (\sigma_u^2 + \sigma_d^2 + 2|\pi|^2) - \sum_{\vec{x}} \sum_a \sum_{m,n} \bar{X}(m, \vec{x}) G^{-1}(m, n; \vec{x}, \phi_a) X(n, \vec{x}), \quad (26)$$

where

$$\bar{X}(m, \vec{x}) = \left(\tilde{u}(m, \vec{x}), \tilde{d}(m, \vec{x}) \right) \quad \text{and} \quad X(n, \vec{x}) = \begin{pmatrix} \tilde{u}(n, \vec{x}) \\ \tilde{d}(n, \vec{x}) \end{pmatrix}, \quad (27)$$

and

$$G^{-1}(m, n; \vec{x}, \phi_a) = \begin{pmatrix} - \left[M_u + i \sin \left(k_m + \frac{\phi_a(\vec{x})}{N_\tau} - i\mu_u \right) \right] \delta_{mn} & i\varepsilon(\vec{x}) \frac{d}{2} \pi^* \delta_{n, m-N_\tau/2} \\ i\varepsilon(\vec{x}) \frac{d}{2} \pi \delta_{n, m-N_\tau/2} & - \left[M_d + i \sin \left(k_m + \frac{\phi_a(\vec{x})}{N_\tau} - i\mu_d \right) \right] \delta_{mn} \end{pmatrix}. \quad (28)$$

$M_u = m + (d/2)\sigma_u$ and $M_d = m + (d/2)\sigma_d$ are the dynamical quark masses of up and down quarks. After performing the integration over the Grassmann variables X and \bar{X} , we obtain the following effective free energy:

$$F_{\text{eff}}[\sigma_u, \sigma_d, \pi; T, \mu_B, \mu_I] = \frac{N_c d}{4} (\sigma_u^2 + \sigma_d^2 + 2|\pi|^2) - T \log \left\{ \int dU_0 \prod_{a=1}^{N_c} \text{Det} [G^{-1}(\phi_a)] \right\}, \quad (29)$$

where

$$\text{Det} [G^{-1}(m, n; \vec{x}, \phi_a)] = \prod_{n=1}^{N_\tau} \left[\left(\frac{d}{2} \right)^2 |\pi|^2 + \{ M_u + i \sin(\bar{k}_n - i\mu_I/2) \} \cdot \{ M_d - i \sin(\bar{k}_n + i\mu_I/2) \} \right] \quad (30)$$

with $\bar{k}_n = k_n + \phi_a(\vec{x})/N_\tau - i\mu_B/N_c$: Here we have rewritten the chemical potentials of the up and down quarks as μ_B and μ_I using the definition $\mu_u = \mu_B/N_c + \mu_I/2$ and $\mu_d = \mu_B/N_c - \mu_I/2$. The integration over U_0 in the Polyakov gauge is defined in Appendix B.

It is impossible to perform the summation over n in Eq. (30) analytically for general μ_B and μ_I . However, we can do it in two interesting cases. One is the case that μ_I is lower than a critical value $\mu_I^{\text{cri}} \sim m_\pi$, where the pion does not condense, $\pi = 0$ [15]. This case is relevant to realistic systems such as heavy ion collisions and electroneutral neutron stars. The other is the case that $\mu_B = 0$, which means we can put $\sigma_u = \sigma_d$. In this case, we can compare our results with those obtained by the recent Monte Carlo lattice simulations [16].

B. The phase structure for $\mu_I < m_\pi$

First, we derive the analytical expression for the effective free energy in the case of $\mu_I < \mu_I^{\text{cri}}$, where we can put $\pi = 0$. The proof for the existence of such a critical value and its correspondence to the pion mass in the framework of strong coupling lattice QCD will be given in the next subsection. In this case, we can calculate the product over n using the formula in Appendix A:

$$\begin{aligned} \text{Det} [G^{-1}(m, n; \vec{x}, \phi_a)] &= \prod_{n=1}^{N_\tau} \{M_u + i \sin [k_n + \phi_a(\vec{x})/N_\tau - i\mu_u]\} \cdot \{M_d + i \sin [k_n + \phi_a(\vec{x})/N_\tau - i\mu_d]\} \\ &= \{2 \cosh [N_\tau E_u] + 2 \cos[\phi_a(\vec{x}) - iN_\tau \mu_u]\} \cdot \{2 \cosh [N_\tau E_d] + 2 \cos[\phi_a(\vec{x}) - iN_\tau \mu_d]\} \end{aligned} \quad (31)$$

with one-dimensional up and down quark excitation energy $E_u = \text{arcsinh} M_u$, $E_d = \text{arcsinh} M_d$.

Using the formula in Appendix B, we can complete the $SU(N_c)$ integration over U_0 in Eq. (29) for general N_c . Then we obtain the analytical expression for the effective free energy as follows:

$$F_{\text{eff}}[\sigma_u, \sigma_d; T, \mu_B, \mu_I < \mu_I^{\text{cri}}] = \frac{N_c d}{4} (\sigma_u^2 + \sigma_d^2) - T \log \left\{ \sum_n \det_{i,j} Q_{n+i-j} \right\}, \quad (32)$$

where

$$\begin{aligned} Q_0 &= 4 \cosh [E_u/T] \cdot \cosh [E_d/T] + 2 \cosh [(\mu_u - \mu_d)/T], \\ Q_{\pm 1} &= 2 \cosh [E_u/T] \cdot (\cosh [\mu_d/T] \pm \sinh [\mu_d/T]) + 2 \cosh [E_d/T] \cdot (\cosh [\mu_u/T] \pm \sinh [\mu_u/T]), \\ Q_{\pm 2} &= \cosh [(\mu_u + \mu_d)/T] \pm \sinh [(\mu_u + \mu_d)/T], \quad Q_{|n| \geq 3} = 0, \end{aligned} \quad (33)$$

and the determinant is to be taken with respect to $i, j = 1, 2, \dots, N_c$.

Although the effective free energy has a complicated expression, it reduces to a simple form at $T = 0$. In the zero temperature limit $N_\tau \rightarrow \infty$, the contribution of $\phi_a(\vec{x})$ in Eq. (31) vanishes. Then the up quarks and the down quarks are completely decoupled, and we can write the effective free energy for $T = 0$ as

$$F_{\text{eff}}[\sigma; T = 0, \mu_B, \mu_I < \mu_I^{\text{cri}}] = \left[\frac{N_c d}{4} \sigma_u^2 - \max \{N_c \mu_u, N_c E_u\} \right] + \left[\frac{N_c d}{4} \sigma_d^2 - \max \{N_c \mu_d, N_c E_d\} \right]. \quad (34)$$

Each term coincides with the effective free energy at $T = 0$ for $N_f = 4$ [Eq. (18)] with quark chemical potential μ_u or μ_d . Therefore the discussions on chiral restoration at finite density given in Sec. II B hold true in each sector.

The phase diagrams

At finite temperature, the integration over the temporal gauge link variable ϕ_a of Eq. (31) nontrivially couples the up and down quark sectors. Let us see its consequences numerically here. We show in Fig. 3 the phase diagram in the plane of T and μ_B with $N_f = 8$, determined by minimizing the effective free energy Eq. (32) for $N_c = 3$, $d = 3$ with respect to the order parameters σ_u, σ_d .

First we consider the case of $\mu_I = 0$ in which we can put $\sigma_u = \sigma_d$; the phase diagram is shown in the left panel of Fig. 3. This should be compared to the case of four-flavor QCD in Fig. 2. The outline of the phase diagrams is quite consistent, and the discussions given in Sec. II C hold true here, while the critical temperature for $N_f = 8$ flavor is lower than that for $N_f = 4$. This is expected from a physical point of view: With more flavors, the chiral condensate is broken faster by their thermal excitations. In other words, the critical temperature decreases on increasing the number of quark flavors. What we want to emphasize here is that the integration over ϕ_a causes the N_f dependence of the critical temperature even at the mean field level.

Next we consider the phase diagram at $\mu_I = 0.2$ with $m = 0.4$. As shown in the right panel of Fig. 3, the introduction of μ_I splits the first order phase transition line into two lines associated with the jump of the chiral condensate of the up quark and that of the down quark. They shift in opposite directions of μ_B and terminate at the second order critical end points. Such a successive chiral restoration with finite μ_I on increasing μ_B is easy to understand intuitively from the fact that up and down quarks experience the chemical potential differently, $\mu_u = \mu_B/N_c + \mu_I/2$ and $\mu_d = \mu_B/N_c - \mu_I/2$.

What is nontrivial in our result is the position of the critical end points. The temperatures of the critical end points for σ_u and σ_d are both higher than that in the case of $\mu_I = 0$. This is in contrast to studies using the random matrix

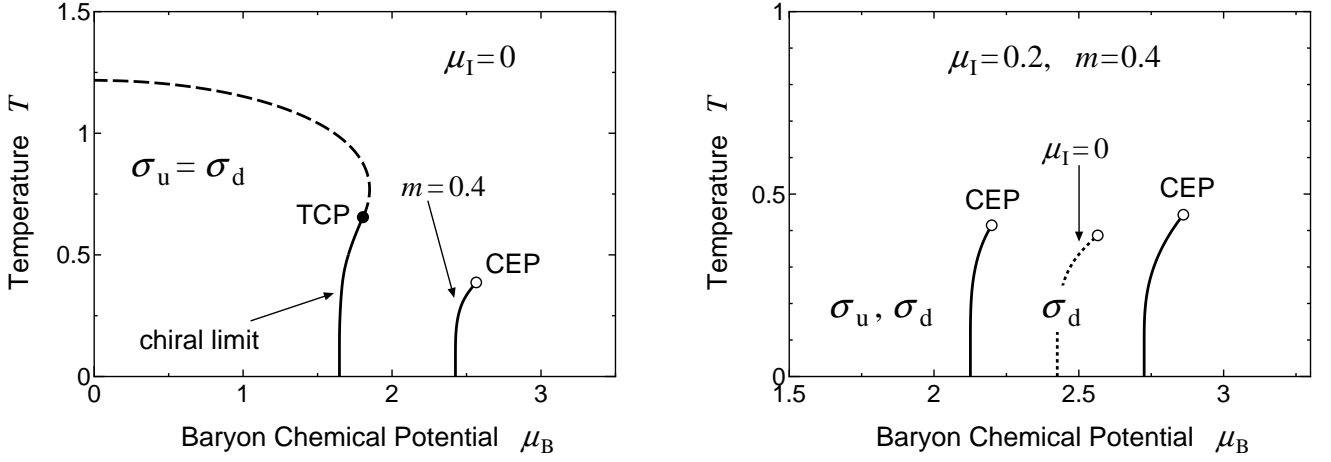


FIG. 3: Phase diagrams of strong coupling lattice QCD with $N_c = 3, N_f = 8$ in the T - μ_B plane with zero (the left panel) and finite (the right one) isospin chemical potential μ_I . In the left panel, the solid (dashed) line denotes the phase transition line for the first (second) order phase transition in the chiral limit at $\mu_I = 0$. The first order line and its critical end point for $m = 0.4$ are also shown. The right panel shows the phase diagram at $\mu_I = 0.2$ and $m = 0.4$. The two solid lines represent the phase transition lines for the first order phase transitions associated with up (the left line) and down (the right one) quark condensates, respectively. The first order phase transition line for $\mu_I = 0$ is plotted by the dotted line for comparison. The symbol σ_u or σ_d in the figure represents the region where the condensate has a large value.

model [35], Nambu–Jona-Lasinio model [36] and ladder QCD approach [37], where the temperature of the critical end points is not affected by μ_I because the up quark sector and the down quark sector are completely uncoupled in such approaches. In our approach, as discussed above, the up and down quarks are nontrivially coupled via the integration of the temporal gauge link variable U_0 at finite temperature.

C. The phase structure for $\mu_B = 0$

We derive the analytical expression for the effective free energy in the case of $\mu_B = 0$. In this case, we can put $\sigma = \sigma_u = \sigma_d$ and obtain the following expression for Eq. (30):

$$\text{Det} [G^{-1}(m, n; \vec{x}, \phi_a)] = \prod_{n=1}^{N_\tau} \left[\left(\frac{d}{2} \right)^2 |\pi|^2 + \left\{ M + i \sin \left(k_n + \frac{\phi_a(\vec{x})}{N_\tau} - i \frac{\mu_I}{2} \right) \right\} \cdot \left\{ M - i \sin \left(k_n + \frac{\phi_a(\vec{x})}{N_\tau} + i \frac{\mu_I}{2} \right) \right\} \right]. \quad (35)$$

This expression has the same form as the determinant calculated in [23] for $SU_c(2)$ QCD. Therefore we can use the formula in the Appendix of [23] for the product over the Matsubara frequencies, and then we obtain

$$\text{Det} [G^{-1}(m, n; \vec{x}, \phi_a)] = \{2 \cosh [N_\tau E_-] + 2 \cos [\phi_a(\vec{x})]\} \cdot \{2 \cosh [N_\tau E_+] + 2 \cos [\phi_a(\vec{x})]\} \quad (36)$$

with one-dimensional up quark and down antiquark (or up antiquark and down quark) excitation energy

$$E_\pm = \text{arccosh} \left(\sqrt{(1 + M^2) \cosh^2 [\mu_I/2] + (d/2)^2 |\pi|^2 \pm M \sinh [\mu_I/2]} \right). \quad (37)$$

Using the formula in Appendix B, we can complete the $SU(N_c)$ integration over U_0 in Eq. (29) for general N_c . Then we obtain the analytical expression for the effective free energy as follows:

$$F_{\text{eff}}[\sigma, \pi; T, \mu_B = 0, \mu_I] = \frac{N_c d}{2} (\sigma^2 + |\pi|^2) - T \log \left\{ \sum_n \det_{i,j} R_{n+i-j} \right\}, \quad (38)$$

where

$$\begin{aligned} R_0 &= 4 \cosh [E_-/T] \cdot \cosh [E_+/T] + 2, \\ R_{\pm 1} &= 2 \cosh [E_-/T] + 2 \cosh [E_+/T], \\ R_{\pm 2} &= 1, \quad R_{|n| \geq 3} = 0, \end{aligned} \quad (39)$$

and the determinant is to be taken with respect to $i, j = 1, 2, \dots, N_c$. Note that for $m = 0$ and $\mu_I = 0$, the effective free energy is a function of only $\sigma^2 + |\pi|^2$. Of course, this is from the chiral symmetry $U(2)_A$ of the original action at $m = \mu_I = 0$. The symmetry between σ and π will play an important role in understanding numerical results on the phase structure.

Although the effective free energy has a complicated expression, it reduces to a simple form at $T = 0$. In the zero temperature limit $N_\tau \rightarrow \infty$, the contribution of $\phi_a(\vec{x})$ in Eq. (36) vanishes, and we obtain the effective free energy for $T = 0$ as

$$F_{\text{eff}}[\sigma, \pi; T = 0, \mu_B = 0, \mu_I] = N_c \left[\frac{d}{2} (\sigma^2 + |\pi|^2) - (E_- + E_+) \right]. \quad (40)$$

If we replace π by Δ and μ_I by μ_B , the above expression corresponds to the free energy at $T = 0$ of $SU_c(2)$ QCD studied in [23] up to the overall factor N_c . This correspondence is rather natural from the point of view of the symmetry and the effect of the chemical potential. In the present system, up and down quarks are indistinguishable because of chiral symmetry at $\mu_I = 0$ and they undergo the effect of μ_I with opposite signs. On the other hand, in $SU_c(2)$ QCD, the quark and antiquark are indistinguishable because of the Pauli-Gürsey symmetry [38] at $\mu_B = 0$, and they also undergo the effect of μ_B with opposite signs. Therefore there is a correspondence between the up (down) quark in the finite isospin density system and the (anti)quark in the finite baryon density $SU_c(2)$ system, which also means a correspondence between the pion condensation and the diquark condensation. Note that the difference of the effective free energy in the two systems at $T \neq 0$ is due to the integration of U_0 for the finite isospin density system, which couples up and down quarks nontrivially at finite temperature.

As calculated in [23] for the case of $SU_c(2)$ QCD, we can derive analytical properties from the effective free energy at $T = 0$ in Eq. (40). The system has two critical chemical potentials, the lower one μ_c^{low} and the upper one μ_c^{up} , given, respectively, by

$$\mu_c^{\text{low}} = 2 \operatorname{arccosh} \sqrt{1 + mM} \quad \text{and} \quad \mu_c^{\text{up}} = 2 \operatorname{arccosh} \sqrt{1 + K^2}, \quad (41)$$

where M is a solution of the chiral gap equation with quark mass m , and we have defined K as the solution of the equation

$$\frac{2}{d} \left(K - \frac{m^2}{K} \right) = (1 + K^2)^{-1/2}. \quad (42)$$

The nonvanishing value of the pion condensate $\pi \neq 0$ is possible only for $\mu_c^{\text{low}} \leq \mu_I \leq \mu_c^{\text{up}}$. As long as $\mu_I < \mu_c^{\text{low}}$, the empty vacuum gives $\rho_I = -\partial F_{\text{eff}}/\partial \mu_I = 0$ and $\pi = 0$. On the other hand, for $\mu_I > \mu_c^{\text{up}}$, saturation of the isospin density occurs, leading to $\rho_I = N_c$ and $\pi = 0$. For sufficiently small m , the lower critical chemical potential reduces to

$$\mu_c^{\text{low}} = 2 m^{1/2} \cdot \left\{ \frac{(1 + d^2)^{1/2} - 1}{2} \right\}^{1/4}. \quad (43)$$

This expression can be rewritten as $\mu_c^{\text{low}} = m_\pi$ with m_π being the pion mass obtained from the excitation spectrum in the vacuum [28] up to leading order of the $1/d$ expansion. This is nothing but a proof of the fact that the critical value of the isospin chemical potential μ_I^{cri} assumed in the previous subsection indeed exists and corresponds to the pion mass.

Condensates and isospin density

Now we determine the chiral condensate σ and the pion condensate π numerically by minimizing the effective free energy with $N_f = 8$ flavors in Eq. (38) for $N_c = 3$, $d = 3$. The isospin density $\rho_I = -\partial F_{\text{eff}}/\partial \mu_I$ is also calculated as a function of μ_I and T . The results are shown in Fig. 4 for $m = 0$ and $m = 0.02$. Here we choose π to be real.

Let us first consider σ , π and ρ_I as functions of μ_I at $T = 0$, shown in the left panels of Fig. 4. In the chiral limit $m = 0$ (the upper left panel), σ is always zero, while π decreases monotonically as a function of μ_I and shows a second order transition when μ_I becomes of order 2. On the other hand, ρ_I increases until the saturation point $\rho_I = 3$ where quarks occupy the maximally allowed configurations by the Fermi statistics.

The lower left panel of Fig. 4 is the result for small quark mass $m = 0.02$. As we discussed above, there exists a lower critical chemical potential $\mu_c^{\text{low}} \sim m_\pi$ given by Eq. (41). Both π and ρ_I start to take finite values only for $\mu_I > \mu_c^{\text{low}}$. One can view the behavior of σ and π with finite quark mass as the manifestation of two different

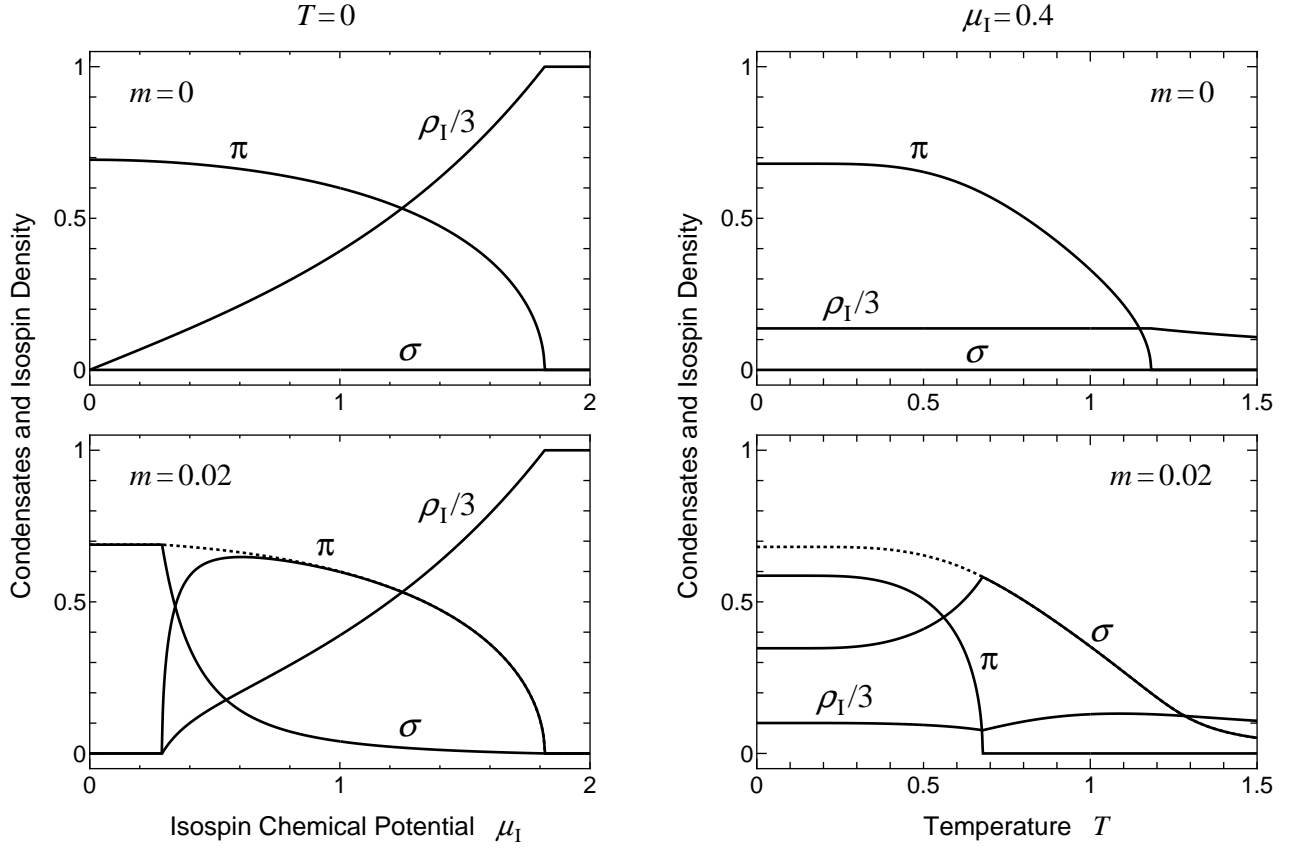


FIG. 4: Chiral condensate σ , pion condensate π and isospin density ρ_I for $N_c = 3, N_f = 8$. In the left panels, they are plotted as functions of the isospin chemical potential μ_I at $T = 0$ for $m = 0$ (the upper panel) and $m = 0.02$ (the lower one). In the right panels, they are plotted as functions of the temperature T at $\mu_I = 0.4$ for $m = 0$ (the upper panel) and $m = 0.02$ (the lower one). The dotted lines in the lower panels indicate the total magnitude of the condensates $\sqrt{\sigma^2 + \pi^2}$.

mechanisms. One is a continuous “rotation” from chiral condensation to pion condensation above $\mu_I = \mu_c^{\text{low}}$ with $\sqrt{\sigma^2 + \pi^2}$ varying smoothly. The other is the “saturation effect”; the isospin density forces the pion condensate to decrease and disappear for large μ_I as seen in the previous case of $m = 0$.

The “rotation” can be understood as follows. As we have discussed, the effective free energy at vanishing m and μ_I has a chiral symmetry between the chiral condensate and the pion condensate. The effect of m (μ_I) is to break this symmetry in the direction of the chiral (pion) condensation favored. Therefore at finite m a relatively large σ appears predominantly for the small μ_I region. Once μ_I exceeds a threshold value μ_c^{low} , σ decreases while π increases, because the effect of μ_I surpasses that of m . As μ_I becomes larger, the pion condensate begins to decrease in turn by the effect of the “saturation” and eventually disappears when μ_I exceeds the upper critical value μ_c^{up} (of the order of 2 for $T = 0$). Such a behavior of π is also observed in recent Monte Carlo simulations of the same system [16].

Next we consider the chiral and pion condensates as functions of T at $\mu_I = 0.4$ in the right panels of Fig. 4. In the chiral limit $m = 0$ (the upper right panel), σ is always zero, while π decreases monotonically and shows a second order phase transition at some critical temperature T_c .

For small quark mass $m = 0.02$ (the lower right panel), both σ and π have finite values. π decreases monotonically as T increases and shows a second order phase transition at a critical temperature smaller than for $m = 0$. On the other hand, σ increases as π decreases, so that the total condensate $\sqrt{\sigma^2 + \pi^2}$ is a smoothly varying function of T . The understanding based on the approximate symmetry between the chiral and pion condensates is thus valid. An interesting observation is that σ , although it is a continuous function of T , has a cusp shape associated with the phase transition of the pion condensate.

Finally let us compare the results for $m = 0$ and those for $m = 0.02$ in Fig. 4. Looking at the two figures at the same T or μ_I , we find that the pion condensate π for $m = 0$ and the total condensate $\sqrt{\sigma^2 + \pi^2}$ for $m = 0.02$ have almost the same behavior. This indicates that, although the current quark mass suppresses π , the price to pay is an

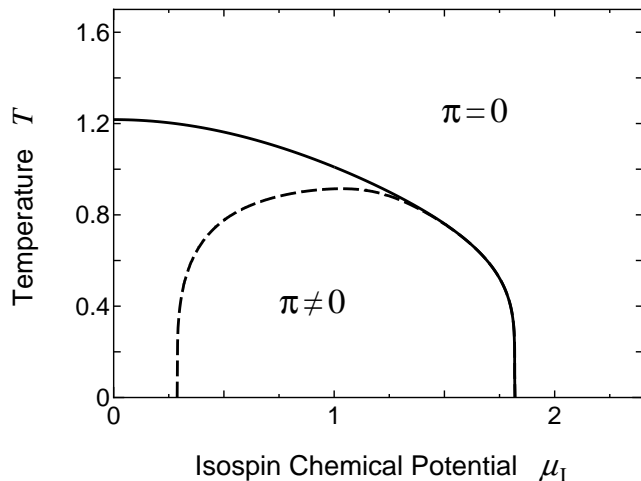


FIG. 5: Phase diagram of strong coupling lattice QCD with $N_c = 3, N_f = 8$ in the T - μ_I plane. The solid (dashed) line denotes the second order critical line for pion condensation for $m = 0$ ($m = 0.02$).

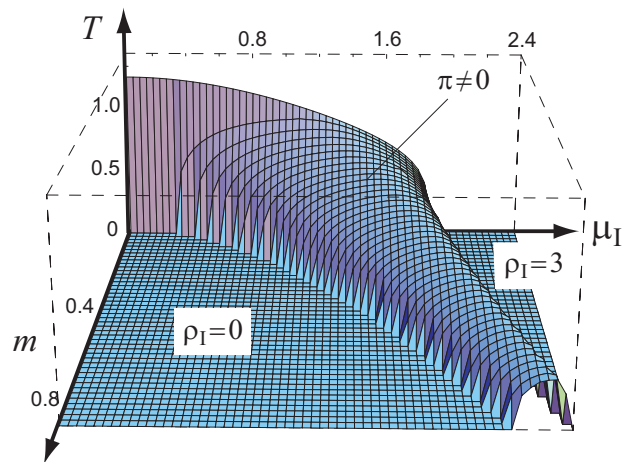


FIG. 6: Phase structure of strong coupling lattice QCD with $N_c = 3, N_f = 8$ in the T - μ_I - m space. The surface represents the critical surface for pion condensation, which separates the region where $\pi \neq 0$ (inside) from the region where $\pi = 0$ (outside).

increase in σ , so as to make the total condensate insensitive to the presence of small m .

The phase diagrams

Now we show in Fig. 5 the phase diagram of the strong coupling lattice QCD with $N_c = 3, N_f = 8$ in the T - μ_I plane. The solid line denotes the critical line separating the pion condensation phase $\pi \neq 0$ from the normal phase $\pi = 0$ in the chiral limit $m = 0$ and the dashed line is for small quark mass $m = 0.02$. The phase transition is of second order on these critical lines. The chiral condensate σ is everywhere zero for $m = 0$, while it is everywhere finite for $m \neq 0$. In the latter case, however, σ is particularly large in the region between the solid line and the dashed line.

Then the phase structure in the three dimensional T - μ_I - m space is shown in Fig. 6. The pion condensate has a nonvanishing value inside the critical surface and the phase transition is of second order everywhere on this critical surface. The second order phase transition is consistent with other analyses employing the mean field approximation [35, 39]. On the other hand, Monte Carlo simulations of QCD with finite μ_I [16] show an indication of the presence of a tricritical point in the T - μ_I plane at which the property of the phase transition line changes from second order to first order as μ_I increases. Clarifying what induces such a first order phase transition is an interesting open problem.

The plane at $T = 0$ in Fig. 6 shows the phase diagram in terms of μ_I and m . The lower left of the plane corresponds to the vacuum with no isospin density present, $\rho_I = 0$. On the other hand, the upper right of the plane corresponds to the saturated system, $\rho_I = 3$, in which every lattice site is occupied by three pions. There is a pion condensation phase (a superfluid phase of isospin charge) with $\pi \neq 0$ and $0 < \rho_I < 3$ bounded by the above two limiting cases. They are separated by the two critical lines given in Eq. (41).

It is worth mentioning here that we can see the corresponding system in the context of condensed matter physics; the hard-core boson Hubbard model has a similar phase diagram in which a superfluid phase is sandwiched by Mott-insulating phases with zero or full density [40]. Here we can give a physical explanation for the saturation effect, that is, why the saturated isospin density forces the pion condensate to disappear. Suppose that one imposes a small external field for the isospin charge on the system in which every lattice site is occupied maximally by pions. However, a pion at one site cannot hop to the next site, owing to the Pauli principle of constituent quarks, and thus the isospin current never appears. This results in a zero condensate because the superfluid current is proportional to the square of the absolute value of the condensate. This is nothing but an analogous phenomenon to the Mott insulator.

The fact that $SU_c(3)$ QCD at finite isospin density has the same phase structure as that of $SU_c(2)$ QCD at finite baryon density can be understood from the aspect of the symmetry and its breaking pattern. $SU_c(3)$ QCD at $\mu_I = 0$ and $m = 0$ has chiral symmetry between the chiral condensate and the pion condensate. On the other hand, $SU_c(2)$ QCD at $\mu_B = 0$ and $m = 0$ has Pauli-Gürsey symmetry between the chiral condensate and the diquark condensate. In both theories, the introduction of m breaks the symmetries so that the chiral condensate is favored, and the

introduction of μ_I/μ_B breaks the symmetries so that the pion/diquark condensate is favored. This is the reason why these two theories have similar phase structures at finite density.

IV. SUMMARY AND DISCUSSION

In this paper, we studied the phase structure of hot and dense QCD with $N_c = 3$ and $N_f = 4, 8$ in the strong coupling limit, formulated on a lattice. We employed the $1/d$ expansion (only in the spatial direction) and the mean field approximation to derive the free energy written in terms of the chiral condensate σ and the pion condensate π at finite temperature T , baryon chemical potential μ_B , isospin chemical potential μ_I and quark mass m .

In Sec. II, we investigated the phase structure with $N_f = 4$ in the T - μ_B plane, and the phase transition of chiral restoration was found to be of second order in the high temperature region and of first order in the low temperature region. Analytical formulas for the critical line of the second order transition and the position of the tricritical point were derived. The critical temperature at small quark chemical potential $\mu = \mu_B/N_c$ can be expanded as $T_c(\mu) \simeq T_c(0) - 1.5\mu^2/T_c(0)$, and the slope was found to be much larger than that calculated in Monte Carlo lattice simulations [9, 10, 11, 12]. We discussed how this difference could be understood as a result of the strong coupling limit $g \rightarrow \infty$ and the chiral limit $m = 0$. We also studied the effect of finite quark mass on the phase diagram: The position of the critical end point has a relatively large dependence on the quark mass. In particular for small m , the critical end point shifts in the direction of smaller T and smaller μ_B . This is because the gradient of the phase transition line near the tricritical point is positive; how this feature in the phase diagram of QCD is affected by the introduction of dynamical baryons beyond the leading order of the $1/d$ expansion should be studied in future work.

In Sec. III, we derived the free energy including μ_I by extending the formulation studied in Sec. II with two species of staggered fermion ($N_f = 8$). First, we observed that the critical temperature of chiral restoration decreases on increasing the number of quark flavors due to the thermal excitations of mesons. Then we studied the effect of μ_I on the phase diagram in the T - μ_B plane at finite quark mass: The introduction of μ_I splits and shifts the first order phase transition line in opposite directions of μ_B . In addition, μ_I moves the two critical end points to higher temperatures than that for $\mu_I = 0$. This is a nontrivial effect originating from integration over the temporal gauge link variable at finite temperature, which couples the up and down quark sectors.

Finally, we studied the phase structure in the space of T , μ_I and m and found a formal correspondence between color $SU_c(3)$ QCD with finite isospin density and color $SU_c(2)$ QCD with finite baryon density. Such a correspondence can be understood by considering the symmetry and its breaking pattern: chiral (Pauli-Gürsey) symmetry at $m = 0$ and $\mu_I = 0$ ($\mu_B = 0$) is broken by the quark mass in the direction of chiral condensation, while it is broken by the isospin (baryon) chemical potential in the direction of pion (diquark) condensation. Although our results are in principle limited to strong coupling, the behavior of σ , π , and ρ_I in the T - μ_I - m space has qualitative agreement with recent lattice data. We also found that the disappearance of pion condensation with saturated density can be understood as a Mott-insulating phenomenon.

The remaining work to be explored is to investigate the phase structure with finite μ_B and finite μ_I as well as with T and m , where a nontrivial competition between the chiral and pion condensates takes place. In our formulation, such a study is possible by using the effective free energy given in Eq. (29) with numerical summation over the Matsubara frequency and numerical integration over the temporal gauge link variable. How the chiral condensate at finite μ_B is replaced by the pion condensate as μ_I increases is one of the most interesting problem to be examined.

Acknowledgments

The author is grateful to T. Hatsuda, K. Fukushima and S. Sasaki for continuous and stimulating discussions on this work and related subjects. He also thanks S. Hands for discussions on the parity transformation of staggered fermions.

APPENDIX A: SUMMATION OVER THE MATSUBARA FREQUENCY

In this appendix, we give the formula for the product over the Matsubara frequencies of the expression

$$I = \prod_{n=1}^{N_\tau/2} [\sin^2 \bar{k}_n + \lambda^2] = \prod_{n=1}^{N_\tau} [\sin^2 \bar{k}_n + \lambda^2]^{1/2} \quad (\text{A1})$$

with $\bar{k}_n = 2\pi(n-1/2)/N_\tau + \phi/N_\tau - i\mu$ and N_τ an even integer. Let us first take the logarithm of the above expression and differentiate it with respect to λ :

$$\frac{\partial}{\partial \lambda} \log I = \sum_{n=1}^{N_\tau} \frac{\lambda}{\sin^2 \bar{k}_n + \lambda^2}. \quad (\text{A2})$$

Because $\sin(k_n + \phi/N_\tau - i\mu)$ is invariant under the shift $n \rightarrow n + N_\tau$, we can make the summation of n over the range $n = -\infty$ to $n = +\infty$ with an appropriate degeneracy factor Ω . Then the residue theorem enables us to replace the summation by a complex integral as

$$\frac{\partial}{\partial \lambda} \log I = \frac{1}{\Omega} \left[\oint \frac{dz}{2\pi i} \frac{\lambda}{\sin^2(z + \phi/N_\tau - i\mu) + \lambda^2} \frac{-iN_\tau}{1 + e^{iN_\tau z}} - \sum_{\bar{z}} \frac{\lambda}{2 \sin(\bar{z} + \phi/N_\tau - i\mu) \cos(\bar{z} + \phi/N_\tau - i\mu)} \frac{-iN_\tau}{1 + e^{iN_\tau \bar{z}}} \right]. \quad (\text{A3})$$

Owing to the infinite range of the summation over n , we can choose the closed contour at infinity for the complex integrals with respect to z , and thus such complex integrals go to zero. \bar{z} are the residues satisfying

$$\sin^2(\bar{z} + \phi/N_\tau - i\mu) + \lambda^2 = 0. \quad (\text{A4})$$

Solving this equation, we obtain

$$\bar{z} + \phi/N_\tau - i\mu = \pm iE + 2\pi n, \quad \pm iE + \pi + 2\pi n, \quad (\text{A5})$$

with $E = \text{arcsinh} \lambda$ and $n = -\infty, \dots, \infty$. Substituting Eq. (A5) into Eq. (A3), we obtain

$$\begin{aligned} \frac{\partial}{\partial \lambda} \log I &= \frac{1}{\Omega} \sum_{n=-\infty}^{\infty} \frac{1}{\cosh E} \left[\frac{N_\tau}{1 + e^{-N_\tau E - i\phi - N_\tau \mu}} - \frac{N_\tau}{1 + e^{N_\tau E - i\phi - N_\tau \mu}} \right] \\ &= \frac{\partial E}{\partial \lambda} \left[\frac{N_\tau}{1 + e^{-N_\tau E - i\phi - N_\tau \mu}} - \frac{N_\tau}{1 + e^{N_\tau E - i\phi - N_\tau \mu}} \right] \\ &= \frac{\partial}{\partial \lambda} \left[\log \{e^{N_\tau E} + e^{-i\phi - N_\tau \mu}\} + \log \{e^{-N_\tau E} + e^{-i\phi - N_\tau \mu}\} \right] \\ &= \frac{\partial}{\partial \lambda} \left(-i\phi - N_\tau \mu + \log \{2 \cosh [N_\tau E] + 2 \cos[\phi - iN_\tau \mu]\} \right). \end{aligned} \quad (\text{A6})$$

We note that the degeneracy factor Ω is just canceled by the infinite degeneracy of the summation on n . After integration with respect to λ , we find that the result is expressed in a rather simple form up to irrelevant factors,

$$I = 2 \cosh [N_\tau E] + 2 \cos[\phi - iN_\tau \mu], \quad (\text{A7})$$

with $E = \text{arcsinh} \lambda$.

APPENDIX B: $SU(N_c)$ INTEGRATION IN THE POLYAKOV GAUGE

In this appendix, we give the formula for the $SU(N_c)$ integration

$$J = \int dU_0 F(U_0). \quad (\text{B1})$$

Here we consider the function that can be written as the product of $f(\theta_a)$ in the Polyakov gauge as

$$F(U_0) = \prod_{a=1}^{N_c} f(\theta_a). \quad (\text{B2})$$

Since the $SU(N_c)$ Haar measure in the Polyakov gauge is given by

$$\begin{aligned} \int dU_0 &= \int_{-\pi}^{\pi} \prod_{a=1}^{N_c} \frac{d\phi_a}{2\pi} \prod_{a < b} |e^{i\phi_a} - e^{i\phi_b}|^2 \Big|_{\sum_a \phi_a = 0} \\ &= \int_{-\pi}^{\pi} \prod_{a=1}^{N_c} \frac{d\phi_a}{2\pi} \left| \epsilon_{i_1 \dots i_{N_c}} e^{i\phi_1(N_c - i_1)} \dots e^{i\phi_{N_c}(N_c - i_{N_c})} \right|^2 \cdot 2\pi \delta \left(\sum \phi_a \right), \end{aligned} \quad (\text{B3})$$

the integration becomes

$$J = \int_{-\pi}^{\pi} \prod_{a=1}^{N_c} \frac{d\phi_a}{2\pi} \left| \epsilon_{i_1 \dots i_{N_c}} e^{i\phi_1(N_c-i_1)} \dots e^{i\phi_{N_c}(N_c-i_{N_c})} \right|^2 \cdot 2\pi \delta \left(\sum_{a=1}^{N_c} \phi_a \right) \times \prod_{a=1}^{N_c} f(\theta_a). \quad (\text{B4})$$

Because the delta function can be rewritten as

$$2\pi \delta \left(\sum_{a=1}^{N_c} \phi_a \right) = \sum_{n=-\infty}^{\infty} \exp \left[-in \sum_{a=1}^{N_c} \phi_a \right], \quad (\text{B5})$$

we obtain

$$J = \sum_{n=-\infty}^{\infty} \epsilon_{i_1 \dots i_{N_c}} \epsilon_{j_1 \dots j_{N_c}} \prod_{a=1}^{N_c} \int_{-\pi}^{\pi} \frac{d\phi_a}{2\pi} f(\phi_a) \exp[-i(n+i_a-j_a)\phi_a] = N_c! \sum_{n=-\infty}^{\infty} \det_{i,j} M_{n+i-j}. \quad (\text{B6})$$

Here we have defined M_n as

$$M_n = \int_{-\pi}^{\pi} \frac{d\phi}{2\pi} f(\phi) \exp[-in\phi], \quad (\text{B7})$$

and the determinant is to be taken with respect to $i, j = 1, 2, \dots, N_c$.

-
- [1] The latest results at RHIC are in the following:
 PHOBOS Collaboration, B. B. Back *et al.*, Phys. Rev. Lett. **91**, 072302 (2003);
 PHENIX Collaboration, S. S. Adler *et al.*, Phys. Rev. Lett. **91**, 072303 (2003);
 STAR Collaboration, J. Adams *et al.*, Phys. Rev. Lett. **91**, 072304 (2003);
 BRAHMS Collaboration, I. Arsene *et al.*, Phys. Rev. Lett. **91**, 072305 (2003).
- [2] For a recent review on the signal of the quark-gluon plasma, see M. Gyulassy, I. Vitev, X.-N. Wang and B.-W. Zhang, in *Quark-Gluon Plasma 3*, edited by R. C. Hwa and X.-N. Wang (World Scientific, Singapore, 2001), nucl-th/0302077.
- [3] R. Tamagaki, Prog. Theor. Phys. **44**, 905 (1970).
 M. Hoffberg, A. E. Glassgold, R. W. Richardson and M. Ruderman, Phys. Rev. Lett. **24**, 775 (1970).
 For further references, see the review: T. Kunihiro, T. Muto, T. Takatsuka, R. Tamagaki and T. Tatsumi, Prog. Theor. Phys. Suppl. **112**, 1 (1993).
- [4] A. B. Migdal, Nucl. Phys. **A210**, 421 (1972).
 R. F. Sawyer and D.J. Scalapino, Phys. Rev. D **7**, 953 (1973).
 For further references, see T. Kunihiro *et al.* in [3].
- [5] D. B. Kaplan and A. E. Nelson, Phys. Lett. B **175**, 57 (1986).
 For further references, see the review: C. H. Lee, Phys. Rep. **275**, 255 (1996).
- [6] The possibility of superconducting quark matter was originally studied by B. C. Barrois, Nucl. Phys. **B129**, 390 (1977);
 D. Bailin and A. Love, Phys. Rep. **107**, 325 (1984).
 For recent progress on such a system, see K. Rajagopal and F. Wilczek, in *At the Frontier of Particle Physics: Handbook of QCD*, edited by M. Shifman (World Scientific, Singapore, 2001), p. 2061, hep-ph/0011333; M. G. Alford, Annu. Rev. Nucl. Part. Sci. **51**, 131 (2001).
- [7] See, for example, F. Karsch, in *Lectures on Quark Matter*, edited by W. Plessas and L. Mathelitsch (Springer, Berlin, 2002), Lect. Notes Phys. **583**, 209 (2002).
 S. D. Katz, hep-lat/0310051.
- [8] For an introductory review on lattice QCD at finite density and related work, see S. Muroya, A. Nakamura, C. Nonaka and T. Takaishi, Prog. Theor. Phys. **110**, 615 (2003).
- [9] Z. Fodor and S. D. Katz, Phys. Lett. B **534**, 87 (2002); J. High Energy Phys. **03**, 014 (2002).
- [10] C. R. Allton, S. Ejiri, S. J. Hands, O. Kaczmarek, F. Karsch, E. Laermann, Ch. Schmidt and L. Scorzato, Phys. Rev. D **66**, 074507 (2002).
- [11] P. de Forcrand and O. Philipsen, Nucl. Phys. **B642**, 290 (2002); *ibid.* **B673**, 170 (2003).
- [12] M. D'Elia and M.-P. Lombardo, Phys. Rev. D **67**, 014505 (2003).
- [13] S. Hands, J. B. Kogut, M.-P. Lombardo and S. E. Morrison, Nucl. Phys. **B558**, 327 (1999).
 S. Hands, I. Montvay, S. Morrison, M. Oevers, L. Scorzato and J. Skullerud, Eur. Phys. J. C **17**, 285 (2000).
- [14] J. B. Kogut, D. Toublan and D. K. Sinclair, Phys. Lett. B **514**, 77 (2001); Nucl. Phys. **B642**, 181 (2002); Phys. Rev. D **68**, 054507 (2003).
 J. B. Kogut, D. K. Sinclair, S. J. Hands and S. E. Morrison, Phys. Rev. D **64**, 094505 (2001).

- [15] D. T. Son and M. A. Stephanov, Phys. Rev. Lett. **86**, 592 (2001); Phys. At. Nucl. **64**, 899 (2001).
T. D. Cohen, Phys. Rev. Lett. **91**, 032002 (2003); Phys. Rev. Lett. **91**, 222001 (2003).
- [16] J. B. Kogut and D. K. Sinclair, Phys. Rev. D **66**, 014508 (2002); *ibid.* **66**, 034505 (2002).
- [17] P. H. Damgaard, N. Kawamoto and K. Shigemoto, Phys. Rev. Lett. **53**, 2211 (1984); Nucl. Phys. **B264**, 1 (1986)
P. H. Damgaard, D. Hochberg and N. Kawamoto, Phys. Lett. B **158**, 239 (1985).
- [18] E.-M. Ilgenfritz and J. Kripfganz, Z. Phys. C **29**, 79 (1985).
G. Faldt and B. Petersson, Nucl. Phys. **B264** [FS15], 197 (1986).
N. Bilić, K. Demeterfi and B. Petersson, Nucl. Phys. **B377**, 651 (1992).
N. Bilić, F. Karsch and K. Redlich, Phys. Rev. D **45**, 3228 (1992).
- [19] N. Bilić and J. Cleymans, Phys. Lett. B **335**, 266 (1995).
- [20] R. Aloisio, V. Azcoiti, G. Di Carlo, A. Galante and A. F. Grillo, Nucl. Phys. **B564**, 489 (2000).
E. B. Gregory, S.-H. Guo, H. Kröger and X.-Q. Luo, Phys. Rev. D **62**, 054508 (2000).
- [21] Y. Umino, Phys. Rev. D **66**, 074501 (2002).
B. Bringoltz and B. Svetitsky, Phys. Rev. D **68**, 034501 (2003).
V. Azcoiti, G. Di Carlo, A. Galante and V. Laliena, J. High Energy Phys. **0309**, 014 (2003).
S. Chandrasekharan and F.-J. Jiang, Phys. Rev. D **68**, 091501 (2003).
- [22] K. Fukushima, hep-ph/0312057.
- [23] Y. Nishida, K. Fukushima and T. Hatsuda, hep-ph/0306066 to appear in Phys. Rep. (2004).
Y. Nishida, hep-ph/0310160 to appear in Prog. Theor. Phys. Suppl. (2004).
- [24] M. Asakawa and K. Yazaki, Nucl. Phys. **A504**, 668 (1989).
J. Berges and K. Rajagopal, Nucl. Phys. **B538**, 215 (1999).
- [25] M. A. Halasz, A. D. Jackson, R. E. Shrock, M. A. Stephanov and J. J. M. Verbaarschot, Phys. Rev. D **58**, 096007 (1998).
- [26] C. D. Roberts and S. M. Schmidt, Prog. Part. Nucl. Phys. **45**, S1 (2000), and references therein.
T. Ikeda, Prog. Theor. Phys. **107**, 403 (2002).
S. Takagi, Prog. Theor. Phys. **109**, 233 (2003).
- [27] A. Barducci, R. Casalbuoni, S. De Curtis, R. Gatto and G. Pettini, Phys. Rev. D **41**, 1610 (1990).
A. Barducci, R. Casalbuoni, G. Pettini and R. Gatto, Phys. Rev. D **49**, 426 (1994).
- [28] H. Kluberg-Stern, A. Morel and B. Petersson, Nucl. Phys. **B215** [FS7], 527 (1983).
H. Kluberg-Stern, A. Morel, O. Napoly and B. Petersson, Nucl. Phys. **B220** [FS8], 447 (1983).
T. Jolicoeur, H. Kluberg-Stern, A. Morel, M. Lev and B. Petersson, Nucl. Phys. **B235** [FS11], 455 (1984).
- [29] N. Kawamoto and J. Smit, Nucl. Phys. **B192**, 100 (1981).
- [30] C. Van den Doel and J. Smit, Nucl. Phys. **B228**, 122 (1983).
M. F. L. Golterman and J. Smit, Nucl. Phys. **B245**, 61 (1984).
- [31] N. G. Antoniou and A. S. Kapoyannis, Phys. Lett. B **563**, 165 (2003).
- [32] Y. Hatta and T. Ikeda, Phys. Rev. D **67**, 014028 (2003).
- [33] R. D. Pisarski and F. Wilczek, Phys. Rev. D **29**, 338 (1984).
- [34] F. Karsch, C. R. Allton, S. Ejiri, S. J. Hands, O. Kaczmarek, E. Laermann and C. Schmidt, hep-lat/0309116.
- [35] B. Klein, D. Toublan and J. J. M. Verbaarschot, Phys. Rev. D **68**, 014009 (2003).
- [36] M. Frank, M. Buballa and M. Oertel, Phys. Lett. B **562**, 221 (2003).
D. Toublan and J. B. Kogut, Phys. Lett. B **564**, 212 (2003).
- [37] A. Barducci, G. Pettini, L. Ravagli and R. Casalbuoni, Phys. Lett. B **564**, 217 (2003).
- [38] W. Pauli, Nuovo Cimento **6**, 205 (1957).
F. Gürsey, Nuovo Cimento **7**, 411 (1958).
- [39] B. Vanderheyden and A. D. Jackson, Phys. Rev. D **64**, 074016 (2001).
- [40] G. Schmid, S. Todo, M. Troyer and A. Dorneich, Phys. Rev. Lett. **88**, 167208 (2002).